ISSN 1063-7834, Physics of the Solid State, 2017, Vol. 59, No. 11, pp. 2268–2273. © Pleiades Publishing, Ltd., 2017.
Original Russian Text © S.S. Aplesnin, L.V. Udod, M.N. Sitnikov, M.S. Molokeev, L.S. Tarasova, K.I. Yanushkevich, 2017, published in Fizika Tverdogo Tela, 2017, Vol. 59, No. 11, pp. 2246–2251.

SEMICONDUCTORS

Magnetic, Dielectric, and Transport Properties of Bismuth Pyrostannate $Bi_2(Sn_{0.9}Mn_{0.1})_2O_7$

S. S. Aplesnin[a, b], L. V. Udod[a, b, *], M. N. Sitnikov[b], M. S. Molokeev[a], L. S. Tarasova[c], and K. I. Yanushkevich[d]

[a] *Kirensky Institute of Physics, the Federal Scientific Center "Krasnoyarsk Scientific Center," Siberian Branch of Russian Academy of Sciences, Akademgorod 50, Krasnoyarsk, 660036 Russia*

[b] *Reshetnev Siberian State Aerospace University, ul. im. Gazety "Krasnoyarskii rabochii" 31, Krasnoyarsk, 660014 Russia*

[c] *Federal Scientific Center "Krasnoyarsk Scientific Center," Siberian Branch of Russian Academy of Sciences, Akademgorod 50, Krasnoyarsk, 660036 Russia*

[d] *Scientific-and-Practical Materials Research Center, National Academy of Sciences of Belarus, ul P. Brovki 19, Minsk, BY-220072 Republic of Belarus*

**e-mail: luba@iph.krasn.ru*

Received April 11, 2017

Abstract—The effect of replacing manganese ions on the structural, dielectric, transport, and magnetic properties of $Bi_2(Sn_{0.9}Mn_{0.1})_2O_7$ has been studied and the correlation between them has been determined. The change in the type of thermal processes and the thermopower sign upon polymorphous transitions were detected by differential scanning calorimetry. The paramagnetic Curie temperature and the antiferromagnetic interaction were determined in the martensite and austenite phases. The type of current carriers has been established.

DOI: 10.1134/S1063783417110038

1. INTRODUCTION

Compounds with the pyrochlorine structure exhibit various physical properties, including the ferroelectric properties. For example, the phase transition in cadmium pyroniobate $Cd_2Nb_2O_7$ from the paraelectric cubic phase to the pseudo-cubic phase at $T =$ 205 K is accompanied by an anomaly of the permittivity and the appearance of spontaneous polarization [1]. This transition is considered a nonintrinsic ferroelectric transition [2] and sometimes an impurity ferroelastic transition [3]. A doping with iron ions increases this effect [1].

Bismuth pyrochlorine $Bi_2Sn_2O_7$ belongs to a family of pyrochlorine. The crystalline structure of $Bi_2Sn_2O_7$ undergoes several polymorphous transitions, and the monoclinic α-phase is observed to a temperature of 90°C [4]. In [5], it was shown that the polycrystalline samples underwent the $\alpha \rightarrow \beta$ transition at 135°C; domains were detected using the second harmonic method. The results enabled one to suppose that the α-phase and the $\alpha \rightarrow \beta$ transition are ferroelectric. The study of bismuth pyrostannate by the neutron diffraction method showed that the $\beta \rightarrow \gamma$ transition at 626°C occurs as a result of displacements of Bi^{3+} ions. The analysis of X-ray diffraction and neutron diffraction data showed that the α phase is stable below 137°C and belongs to space group $Pc(C_S^2)$. The crystal structure of the α-phase is very complex and contains 176 atoms. At the temperature corresponding to the first phase transition, the unit cell is distorted [6]. The β-phase structure was determined by neutron and synchrotron X-ray diffraction and is cubic with space group $F\bar{4}3c(T_d^s)$ [7].

The $Bi_2Sn_2O_7$ compound is used in gas sensors and multisensors operating in a temperature range to $T =$ 400°C [8]. A possible method of solving the problem of increasing the thermal stability of bismuth stannates limiting possibilities of their practical application and also a change in their electrophysical properties the doping of these compounds with atoms of transition elements [9, 10], which can be promising from the standpoint of their application as multiferroics. Substituting of manganese for tin ions leads to a magnetic ordering and, it is possible, to the appearance of ferroelectric properties. For example, substituted bismuth titanates based on the known ferroelectric $Bi_4Ti_3O_{12}$ are promising as lead-free ferro- and piezoelectric materials [11] and multiferroics. The substitution of titanium for tin ions in the $Bi_2Sn_{2-x}Ti_xO_7$ increases the permittivity and, thus, enhances the electroinsulation characteristics [12].

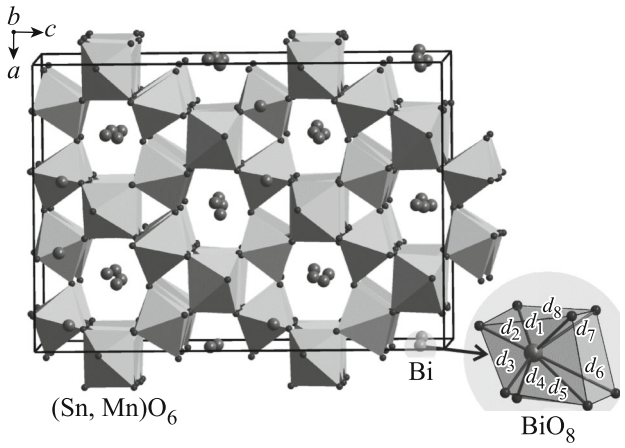

Fig. 1. Crystal structure of $Bi_2(Sn_{0.9}Mn_{0.1})_2O_7$. The inset shows one of 32 independent polyhedrons BiO_8 which form the unit cell. The d_{1-4} bond lengths takes values 2.2–2.5 Å, and the d_{5-8} bond lengths takes values 2.5–3.2 Å.

The aim of this work is to estimate the value of the exchange interaction and the influence of magnetic manganese ions on the structural transitions and the dielectric properties of $Bi_2(Sn_{0.9}Mn_{0.1})_2O_7$. This work continues the series of the studies of the influence of doping of bismuth stannate with chromium ions on the physical properties [9, 10, 13].

2. EXPERIMENTAL

The $Bi_2(Sn_{0.9}Mn_{0.1})_2O_7$ compound was synthesized by the solid-phase reaction method by the following reaction:

$$2(1-x)SnO_2 + 2xMnO_2 + Bi_2O_3 \rightarrow Bi_2(Sn_{1-x}Mn_x)_2O_7.$$

Table 1. Main parameters of $Bi_2(Sn_{0.9}Mn_{0.1})_2O_7$: experiment and the results of the refinement

Parameter	Value
Space group	*Pc*
a, Å	15.097 (1)
b, Å	15.1080 (8)
c, Å	21.378 (1)
β, deg	89.983 (6)
V, Å^3	4875.9 (5)
Range 2θ, deg	5–90
R_{wp}, %	13.06
R_p, %	9.57
R_B, %	5.78
χ^2	1.59

High-purity oxides Bi_2O_3, SnO_2, and MnO_2 were used as initial materials. The initial mixture of the oxides pressed into pellets were placed in a furnace and held at temperatures from 700 to 950°C; the holding time was varied from 8 to 24 h.

The powder X-ray diffraction pattern of $Bi_2(Sn_{0.9}Mn_{0.1})_2O_7$ was obtained at room temperature using a Bruker D8 ADVANCE diffractometer, a VANTEC linear detector, and the CuK_α radiation. All peaks, except several weak impurity peaks of an unknown phase and reflections of impurity phase Bi_2O_3 (3(1)%) corresponded to the *Pc* monoclinic cell of α-phase $Bi_2Sn_2O_7$ [6]. The crystal structure contains 32 Bi^{3+} ion, 32 Sn^{4+} ions, and 112 O^{2-} ions in the independent part of the cell (Fig. 1). All Bi^{3+} ions have eight O^{2-} ions in the nearest environment and form distorted cubes; Sn^{4+} ions are surrounded by six O^{2-} ions and form octahedral connected to each other by tips. The Rietveld refinement was realized using the TOPAS 4.2 program [14]. The coordinates of all 176 atoms were fixed, since the number of coordinate 528 alone is comparable to the number of observed reflections. Nevertheless, even fixed atomic coordinates enabled us to correctly describe all the existing reflections, and the refinement resulted in low unreliability factor (Table 1, Fig. 2). Because the atomic coordinates and thermal parameters were not refined, their values could be taken from [6].

The X-ray diffraction study of $Bi_2(Sn_{0.9}Mn_{0.1})_2O_7$ was carried out both before high-temperature measurements at a temperature to 1000 K and after them. No changes in the positions of the reflections were observed.

The structural transitions were determined by differential scanning calorimetry using a NETZSCH STA 449 C Jupiter unit with a NETZSCH QMS 403 C Aeolos quadrupole mass-spectrometer for analyzing gases released during heating of the samples.

The measurements of the electrical resistance by two-probe method and the thermoelectric coefficient were performed in the temperature range 80–1100 K. The studies were carried out in a continuous regime without remounting the sample. When transiting from the low-temperature to the high-temperature measurements, the cryogenic system was replaced by a heater of a resistance furnace.

The magnetic properties of $Bi_2(Sn_{0.9}Mn_{0.1})_2O_7$ were studied at the high-temperature unit by the Faraday method in the temperature range to 1100 K in magnetic field to 0.86 T.

The dielectric properties of $Bi_2(Sn_{0.9}Mn_{0.1})_2O_7$ were studied using an LCR-829 METER in the temperature range 300–750 K at a frequency of 100 kHz.

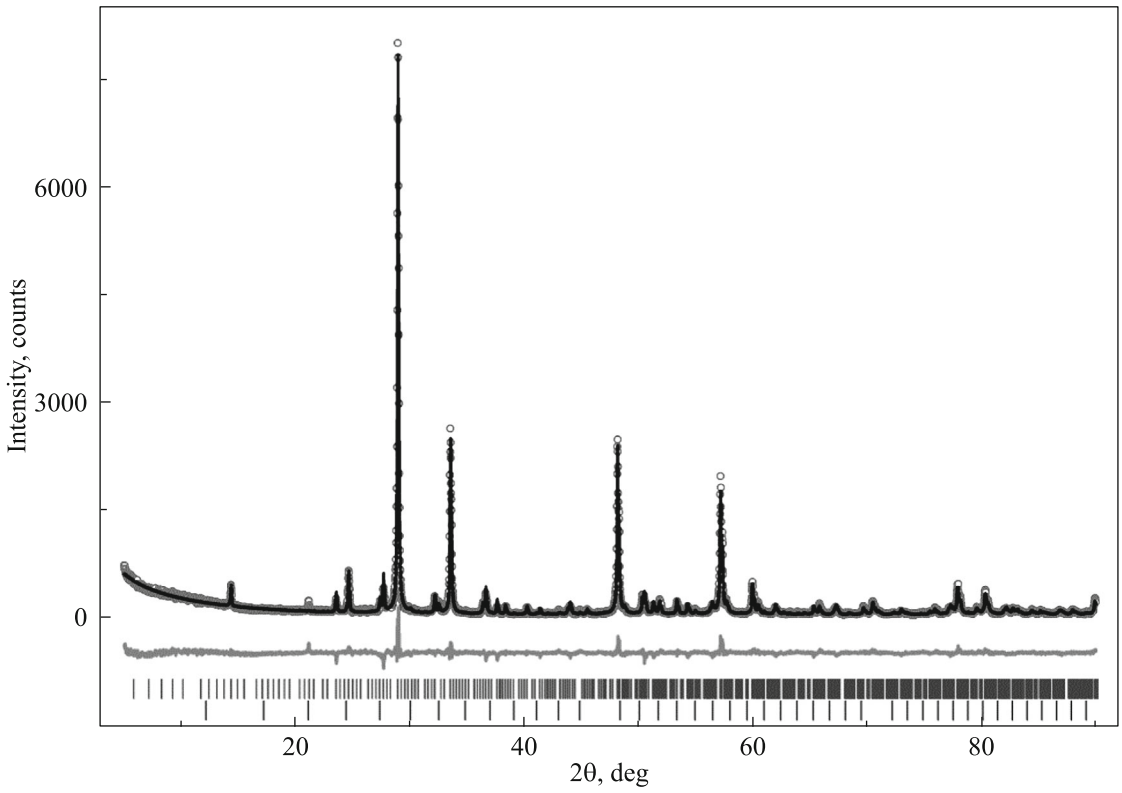

Fig. 2. Difference X-ray diffraction pattern of $Bi_2(Sn_{0.9}Mn_{0.1})_2O_7$.

3. EXPERIMENTAL RESULTS

3.1. Differential Scanning Calorimetry

Figure 3 depicts the results of differential scanning calorimetry (DSC) as the DSC heating curves for three compositions of $Bi_2(Sn_{1-x}Mn_x)_2O_7$: $x = 0$, 0.05, and 0.1. Curve *1* for $Bi_2Sn_2O_7$ demonstrates three endothermic effects at temperatures 370, 548, and 872 K, which indicate the existence of three phase transitions. According to available data [4, 6, 15, 16], $Bi_2Sn_2O_7$ is in the α-phase to ~360 K; therefore, the endothermic peak corresponds to the $\alpha \rightarrow \beta$ transition. It is likely that the $\alpha \rightarrow \beta$ transition passes through two stages, and the transition to the single-phase β-state takes place near $T = 548$ K. The endothermic effect near $T = 872$ K is interpreted as the structural transition to the cubic γ phase.

The heating curve *2* for $Bi_2(Sn_{0.95}Mn_{0.05})_2O_7$ differs from the experimental results for $Bi_2Sn_2O_7$: there is no endothermic effect at 370 K; a weak exothermal effect is observed in this temperature range instead it. It is known that oxygen ions in the pyrochlorine structure are more mobile in the A_2O' [17] (bismuth) sublattice than in the B_2O_6 sublattice. The substitution of manganese for tin ions is likely to change the oxygen partial pressure that manifested itself in the exothermic effect. The initial stage of the $\alpha \rightarrow \beta$ transition observed in $Bi_2Sn_2O_7$ shifted to ~420 K. The temperature range of ~553 K for $Bi_2(Sn_{0.95}Mn_{0.05})_2O_7$ corresponds to the single-phase β-state; in $Bi_2Sn_2O_7$, the polymorphic transformation to the β-phase is accompanied by heat absorption and is described by the endothermic effect at temperature $T = 548$ K (curve *1*, Fig. 3). The proximity of the phase transition temperatures for the compounds with the manganese con-

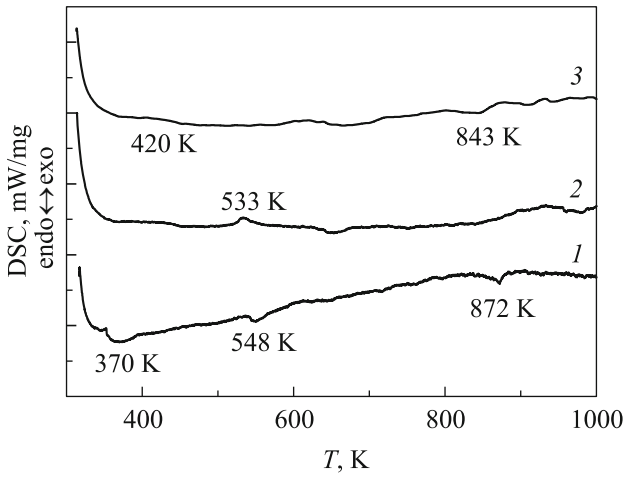

Fig. 3. DSC curves: (*1*) $Bi_2Sn_2O_7$, (*2*) $Bi_2(Sn_{0.95}Mn_{0.05})_2O_7$, and (*3*) $Bi_2(Sn_{0.9}Mn_{0.1})_2O_7$.

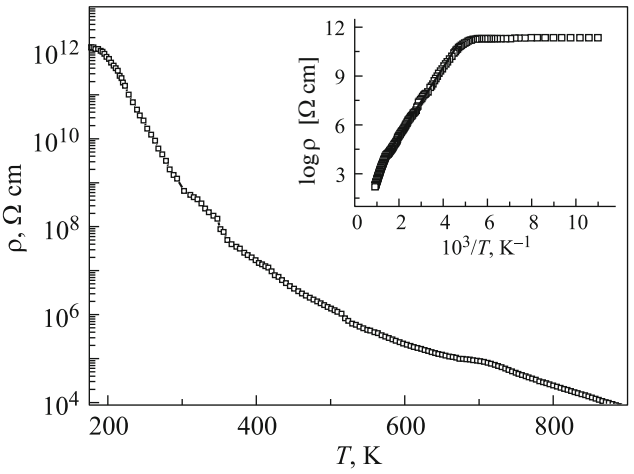

Fig. 4. Temperature dependence of the resistivity of $Bi_2(Sn_{0.9}Mn_{0.1})_2O_7$. The inset shows the temperature dependence of logarithm of the resistivity.

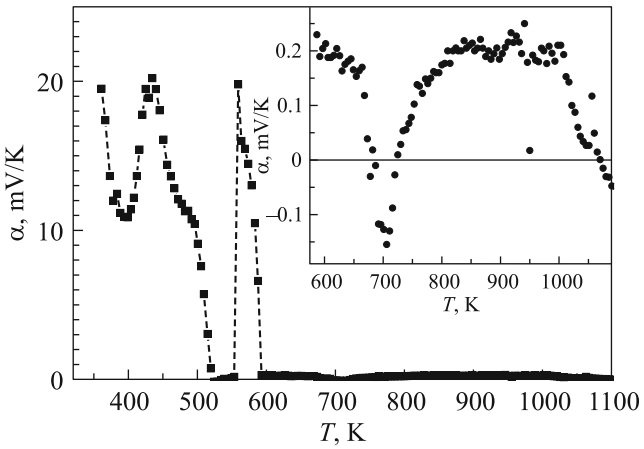

Fig. 5. Temperature dependence of the thermoelectric coefficient of $Bi_2(Sn_{0.9}Mn_{0.1})_2O_7$.

centrations $x = 0$ and 0.05 suggests their similar natures. When manganese doping of bismuth stannate, the formed solid solution $Bi_2(Sn_{0.95}Mn_{0.05})_2O_7$ is likely to be in a metastable state at this temperature and contains an excess energy that releases during transition to the equilibrium β phase. Because of this, we observe the exothermic effect in this case.

The increase of the manganese concentration to $x = 0.1$ led to still further suppression of the thermal effects (curve *3*, Fig. 3). Here, we observed a weak anomaly near $T = 420$ K corresponding to the $\alpha \rightarrow \beta$ transition. At temperatures $T > 843$ K, the compound is in the single-phase cubic state, i.e., γ phase.

3.2. Electrical and Magnetic Properties

Figure 4 shows the temperature dependence of the electrical resistivity measured by the two-probe method. The bulk electrical resistance has a semiconductor character of the conductivity with a weak anomaly of the temperature coefficient of the resistance $(1/R)dR/dT$ in the temperature range, where anomalies were observed in the curves of differential scanning calorimetry.

The activation energy $\Delta E_1 = 0.4$ eV calculated from the dependence of log(ρ on the reciprocal temperature in the range 215–675 K (inset in Fig. 4) was doubled as compared to that of $Bi_2Sn_2O_7$ [18], and it described by a linear function $\ln\rho = \ln\rho_{01} + (\Delta E_1/k_BT)$, where k_B is the Boltzmann constant.

The temperature dependence of the thermoelectric coefficient of $Bi_2(Sn_{0.9}Mn_{0.1})_2O_7$ (Fig. 5) changes its sign form positive to negative two times at $T = 680$ and 1070 K, which indicates the transition from the hole type of the conductivity to the electron type, and has sharp anomalies at $T = 435$ K and 570 K and the wide maximum in the temperature range 850–950 K. These maxima are due to the electron–phonon drag near the structural transitions, where fluctuations of the phase density cause a shift of the potential and induce the electron diffusion.

The phase transitions in $Bi_2(Sn_{0.9}Mn_{0.1})_2O_7$ are accompanied by anomalies of the temperature behavior of the permittivity (Fig. 6). The real part of the permittivity Re(ε) (Fig. 6a) has the inflection point at 418 K and the sharp rise above 700 K. The temperature dependence of the imaginary part of the permittivity Im(ε) (Fig. 6b) has a maximum at $T = 425$ K and a rise starting from $T \sim 700$ K. The anomaly temperatures agree with the temperatures of the extremes in the thermopower and DSC.

The existence of the austenite–martensite transitions is confirmed by the data of magnetic measurements. Figure 7 shows the temperature dependence of the inverse magnetic susceptibility of $Bi_2(Sn_{0.9}Mn_{0.1})_2O_7$ measured on heating (curve *1*) and cooling (curve *2*)

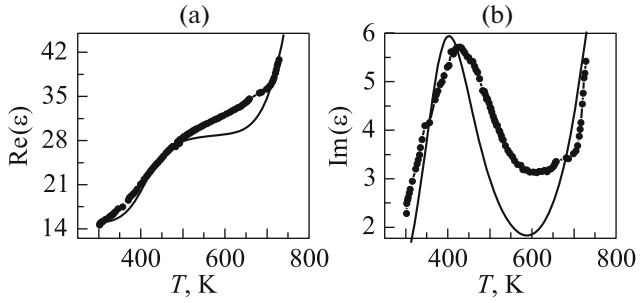

Fig. 6. Temperature dependence of the permittivity of $Bi_2(Sn_{0.9}Mn_{0.1})_2O_7$: (a) temperature dependence of the real part, (b) temperature dependence of the imaginary part. Thin solid lines show the theoretical calculations of the real and imaginary parts of the permittivity in the Debye model.

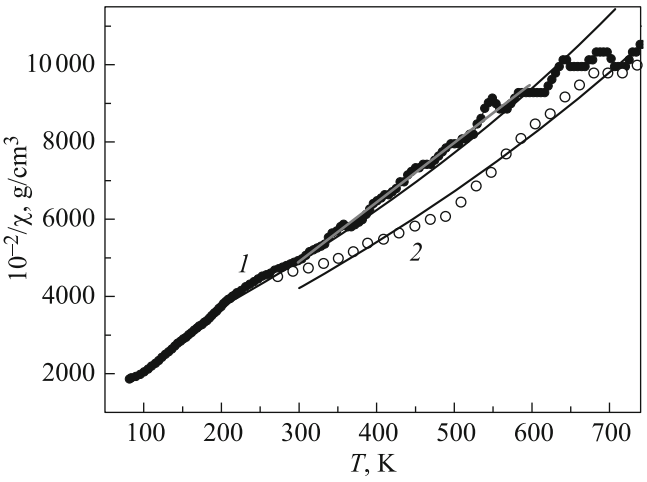

Fig. 7. Temperature dependence of the inverse magnetic susceptibility of $Bi_2(Sn_{0.9}Mn_{0.1})_2O_7$: (*1*) experimental results measured on heating of the sample; the solid curve is the theoretical calculations of $1/\chi^{th}(T)$, $C = -200$ K; (*2*) experimental results measured on cooling of the sample; the solid curve is the theoretical calculations of $1/\chi^{th}(T)$, $C = -150$ K.

of the sample. These curves have two intersection points near temperatures of 270 and 700 K.

4. DISCUSSION

The substitution of manganese ions for tin ions does not change the type of the crystal structure, and the $Bi_2(Sn_{0.9}Mn_{0.1})_2O_7$ compound, as well as $Bi_2Sn_2O_7$ is in the monoclinic *Pc* α phase. The ionic radii of tetravalent tin and manganese are 0.067 and 0.052 nm, respectively, and differ by 25%. The substitution of Mn^{4+} for Sn^{4+} leads to a distortion of the crystal structure, and the structural transition temperatures are shifted to higher temperatures. Manganese ions are in the distorted octahedron of oxygen ions, and 3*d* electrons of Mn^{4+} form an impurity subband.

The temperature dependence of the resistivity does not qualitatively changes as compared to that of $Bi_2Sn_2O_7$. The resistivity of $Bi_2Sn_2O_7$ increases by an order of magnitude near the transition and passes through a maximum at $T = 450$ K; in $Bi_2(Sn_{0.9}Mn_{0.1})_2O_7$, the temperature coefficient of resistance $(1/R)dR/dT$ has a low maximum upon the $\alpha \rightarrow \beta$ transition. Electrons of the manganese ions form potential wells, and the material is characterized by the hopping mechanism of conduction over the manganese ions. The chemical potential is in the region of impurity states, and the change in the crystal structure does not lead to a substantial shift of the chemical potential.

The dielectric susceptibility has a maximum near the structural transition. The relaxation time is described by the Arrhenius function $\tau = \tau_0\exp(\Delta E/kT)$, where ΔE is the activation energy and τ_0 is the proper relaxation time of dipoles. The sample undergoes two structural transitions at $T_1 = 420$ K and $T_2 = 843$ K with the activation energies ΔE_1 and ΔE_2.

The permittivity can be written in the Debye model

$$\mathrm{Re}(\varepsilon) = \varepsilon_0 + \chi_0/(1 + (\omega\tau_1)^2) + \chi_0/(1 + (\omega\tau_2)^2), \quad (1)$$

$$\mathrm{Im}(\varepsilon) = \chi_0\omega\tau_1/(1 + (\omega\tau_1)^2) + \chi_0\omega\tau_2/(1 + (\omega\tau_2)^2), \quad (2)$$

where ε_0 is the temperature-independent contribution to the permittivity, χ_0 is the static susceptibility of dipoles, ω is the frequency, τ_1 and τ_2 are the relaxation times at temperatures T_1 and T_2. The permittivity of $Bi_2(Sn_{0.9}Mn_{0.1})_2O_7$ is well described by functions (1) and (2) shown in Fig. 6 by solid lines with the relaxation times $\tau_1 = \tau_{01}\exp(\Delta E_1/kT)$ and $\tau_2 = \tau_{02}\exp(\Delta E_2/kT)$ and the adjustable parameters $\Delta E_1 = 0.26$ eV, $\tau_{01} = 8 \times 10^{-9}$ s and $\Delta E_2 = 0.69$ eV, $\tau_{02} = 9 \times 10^{-10}$ s.

The contribution of the conduction electrons to the permittivity is absent; since $\mathrm{Im}(\varepsilon(\omega)) = \sigma/\omega$, and the conductivity σ exponentially in the temperature range 300–700 K, the dielectric loss must increase, correspondingly.

The austenite–martensite transitions are observed in the magnetic characteristics. On heating above temperature $T = 300$ K, the magnetic properties of the martensite phase prevail; and on cooling from high temperatures $T = 800$ K, the exchange interactions between manganese ions in the cubic phase (austenite). Similar martensitic transitions are observed in manganites [19]. In the vicinity of 500 K, the magnetic susceptibility measured on cooling is higher by 30% the value measured on heating. The nonlinear temperature dependence of the inverse magnetic susceptibility is provided by the sum of two contributions: paramagnetic and diamagnetic. We represent the resulting susceptibility as

$$\chi(T) = xC/(T + \theta) - \chi_{\mathrm{diam}}, \quad (3)$$

where x is the concentration of paramagnetic atoms (manganese ions), C is the Curie constant, θ is the paramagnetic Curie temperature, and χ_{diam} is the diamagnetic susceptibility. The bismuth ions give the largest diamagnetic contribution; therefore, the diamagnetic susceptibility does not dependent on the heating conditions. The volume diamagnetic susceptibility of bismuth crystals at room temperature is $\chi_{\mathrm{diam}} = -12 \times 10^{-5}$ cm^3/g [20]. When theoretical comparative analyzing the complex susceptibility with the experimental data, the value $\chi_{\mathrm{diam}} = -5 \times 10^{-5}$ cm^3/g was used.

The value of the inverse susceptibility $1/\chi^{th}(T)$ adequately describes the experimental data with $C = 1.36$ K measured on heating and cooling. The effective magnetic moment of $Bi_2(Sn_{0.9}Mn_{0.1})_2O_7$ calculated by

formula $\mu = \sqrt{8C} = 3.3\mu_B$ is smaller by 13% as compared to the theoretical value $\mu_{theor} = 3.8\mu_B$ found from the relationship $\mu_{theor} = g\sqrt{S(S+1)}$, where S is spin of Mn^{4+} ions, $S = 3/2$, $g = 2$. The distortion of the octahedron leads to a decrease in g factor. On heating, when the low-temperature phase prevails, the paramagnetic Curie temperature is $\theta = -200$ K, and, in the high-temperature phase, $\theta = -150$ K. In this temperature range, the electrical resistance of $Bi_2(Sn_{0.9}Mn_{0.1})_2O_7$ varies within 10^4–10^8 Ω; because of this, we can ignore the kinetic exchange of conduction electrons, and the exchange interaction is the result of the indirect exchange of electrons via oxygen anion Mn^{4+}–O^{2-}–Mn^{4+}. The bond angle in pyrochlorines is changed (manganese ions make the chain rectilinear) and is dependent on the crystal symmetry. The exchange value is exponentially dependent on the length of the cation–anion bond. These two factors determine the decrease in the antiferromagnetic interaction in the high-temperature cubic β phase.

5. CONCLUSIONS

The substitution of manganese ions for tin ions changes the type of the thermal effects from the endothermic to the exothermic upon the structural phase transitions and their shift to higher temperatures. The structural $\alpha \rightarrow \beta$ and $\beta \rightarrow \gamma$ are accompanied by the maxima in the temperature behavior of the permittivity. According to the data of the measurement of the thermopower, the material has the hole type of the conduction. The maxima of the thermopower during the structural transitions are due to the electron–phonon drag.

The studies of the temperature behavior of the magnetic susceptibility revealed the martensite-austenite transition accompanied with the temperature hysteresis of the susceptibility. On heating, the low-temperature phase with a higher paramagnetic Curie temperature dominates as compared to the cooling, during which the cubic phase prevails. It is found that the exchange interaction has the antiferromagnetic character and that the effective magnetic moment has the g factor lesser than two.

ACKNOWLEDGMENTS

This work was supported by the Russian Foundation for Basic Researchers, the Government of the Krasnoyarsk Region, the Krasnoyarsk regional Foundation for Support of Scientific and Scientific-Engineering activity in the framework of the scientific projects no. 18-52-00045 Bel_a.

REFERENCES

1. L. S. Kamzina, F. M. Salaev, N. N. Krainik, S. N. Dorogovtsev, and G. A. Smolenskii, Sov. Phys. Solid State **25**, 1645 (1983).
2. F. M. Salaev, L. S. Kamzina, N. N. Krainik, E. S. Sher, and G. A. Smolenskii, Sov. Phys. Solid State **25**, 89 (1983).
3. N. N. Kolpakova, I. G. Sinii, M. Polomska, and A. Petrashko, Sov. Phys. Solid State **24**, 985 (1982).
4. R. D Shannon, J. D. Beirlein, L. J. Gillon, G. A. Jones, and A. W. Sleight, J. Phys. Chem. Solids **41**, 117 (1980).
5. V. Kahlenberg and Th. Zeiske, Z. Kristallogr. **212**, 297 (1997).
6. I. R. Evans, J. A. K. Howard, and J. S. O. Evans, J. Mater. Chem. **13**, 2098 (2003).
7. B. J. Kennedy and I. M. Elcombe, Mater. Sci. Forum **278**, 762 (1998).
8. G. Sarala Devi, S. V. Manoraoma, and V. J. Rao, Sens. Actuators B **56**, 98 (1999).
9. S. S. Aplesnin, L. V. Udod, M. N. Sitnikov, E. V. Eremin, M. S. Molokeev, L. S. Tarasova, K. I. Yanushkevich, and A. I. Galyas, Phys. Solid State **57**, 1627 (2015).
10. S. S. Aplesnin, L. V. Udod, M. N. Sitnikov, and N. P. Shestakov, Ceram. Int. **42**, 5177 (2016).
11. I. A. Zvereva and G. A. Skorobogatov, *Synthetic and Perovskite-Like Layered Oxides: Structure, Synthesis, Properties, Applicatio*n (VVM, St Petersburg, 2009) [in Russian].
12. M. Roy, Indu Bala, and S. K. Barbar, J. Therm. Anal. Calorim. **110**, 559 (2012).
13. L. V. Udod, S. S. Aplesnin, M. N. Sitnikov, E. V. Eremin, and M. S. Molokeev, Solid State Phenom. **233–234**, 105 (2015).
14. *Bruker AXS TOPAS V4: General Profile and Structure Analysis Software for Powder Diffraction Data, User's Manua*l (Bruker AXS, Karlsruhe, Germany, 2008).
15. F. Brisse and O. Knor, Pyrochlores. Can. J. Chem. **46**, 859 (1968).
16. A. Walsh and W. G. Watson, Chem. Mater. **19**, 5158 (2007).
17. T. A. Vanderah, I. Levin, and M. W. Lufaso, Eur. J. Inorg. Chem. **15**, 2895 (2005).
18. L. V. Udod, S. S. Aplesnin, M. N. Sitnikov, and M. S. Molokeev, Phys. Solid State **56**, 1315 (2014).
19. V. Podzorov, B. G. Kim, V. Kiryukhin, M. E. Gershenson, and S-W. Cheong, Phys. Rev. B **64**, 140406(R) (2001).
20. M. E. Drits, P. B. Budberg, G. S. Burkhanov, A. M. Drits, and V. M. Panovko, *Properties of Elements, The Handbook* (Metallurgiya, Moscow, 1985) [in Russian].

Translated by Yu. Ryzhkov